

Atmospheric cooling of freshwater near the temperature of maximum density

Jason Olsthoorn

*Department of Civil Engineering, Queen's University, Kingston, Ontario, Canada, K7L 3N6 **

We perform three-dimensional direct numerical simulations of surface-driven convection near the temperature of maximum density \tilde{T}_{md} . A dynamic surface boundary condition couples heat flux through the surface to the induced convection, creating a dynamic equilibrium between the surface water temperature and the convection below. In this system, we identified three convective regimes: (1) free convection when the surface water temperature is above \tilde{T}_{md} , (2) penetrative convection when the surface water temperature is below \tilde{T}_{md} and the convection is actively mixing the fluid layer, and (3) decaying convection when the convection weakens. We then predict the transitions between these regimes. Understanding these transitions is essential for the predicting timing of ice formation in natural systems.

I. INTRODUCTION

Recent work has highlighted that under-ice thermal stratification plays a key role for the biological dynamics in winter limnology [14]. Moreover, this stratification, which persists through the whole ice-covered period, is largely determined by the thermal structure prior to the formation of lake ice [15]. The two primary processes that control the pre-ice stratification are wind and surface-driven convection. This study is focused on the latter process to understand when convection, driven by atmospheric cooling, will shutdown, enabling the formation of ice.

To account for the heat loss through the air-water interface, Hitchen and Wells [4] and others have demonstrated that the linearized surface boundary flux ($\mathbf{q}_{surf} \cdot \mathbf{n}$) that accounts for longwave radiation, sensible heat flux, and evaporation depends upon the surface water temperature $\tilde{T}_{\tilde{z}=\tilde{H}}$, and is written

$$\mathbf{q}_{surf} \cdot \mathbf{n} = \gamma \left(\tilde{T}_{\tilde{z}=\tilde{H}} - \tilde{T}_R \right), \quad (1)$$

with parameters γ and \tilde{T}_R that depend upon the physical parameters of the system, such as the air temperature, wind speed, and other meteorological variables above the water surface. Olsthoorn [5] then demonstrated that, provided that one takes into account the evolving surface boundary temperature, the magnitude of the heat flux through the water column is consistent with other convective systems. Further, there is an equilibrium surface temperature that results from a balance between the surface cooling that is driving the convection, and the convection-induced warming of the water surface.

One limitation of the previous work of Olsthoorn [5] is that they assumed a linear equation of state. Many systems do not have a linear equation of state. In particular, the equation of state for freshwater is nearly quadratic about the temperature of maximum density ($\tilde{T}_{md} \approx 4$ °C). There has been significant recent research on convection with a nonlinear equation of state [10–12, and others]. One such study by Olsthoorn et al. [6] argued that convection with a quadratic equation of state has two distinct thermal regimes. In the first thermal regime, the bottom water temperature (Θ_B) decays exponentially towards \tilde{T}_{md} with a constant decay rate. Once the convection becomes weak enough, the second thermal regime evolves where the decay rate rapidly decreases. The transition between these two thermal regimes occurred when the ratio of nondimensionalized bottom to surface temperatures $\Theta_B < -C_3\Theta_S$, for some constant C_3 . However, Olsthoorn et al. [6] used a fixed surface temperature, which does not account for the dynamic heat loss through the air-water interface.

This paper builds upon both Olsthoorn [5] and Olsthoorn et al. [6] to study the induced convection as water approaches \tilde{T}_{md} . To that end, we investigate convection with a quadratic equation of state using the linearized surface boundary condition (1). We aim to determine: first, how rapidly does the water temperature decrease and second, when does convection shut down in this system.

The remainder of this paper is organized as follows: we continue in §II with a discussion of the numerical methods and specific cases performed. We then discuss each of the objectives in turn in §III A–III B, before finally concluding in §IV

* Jason.Olsthoorn@queensu.ca

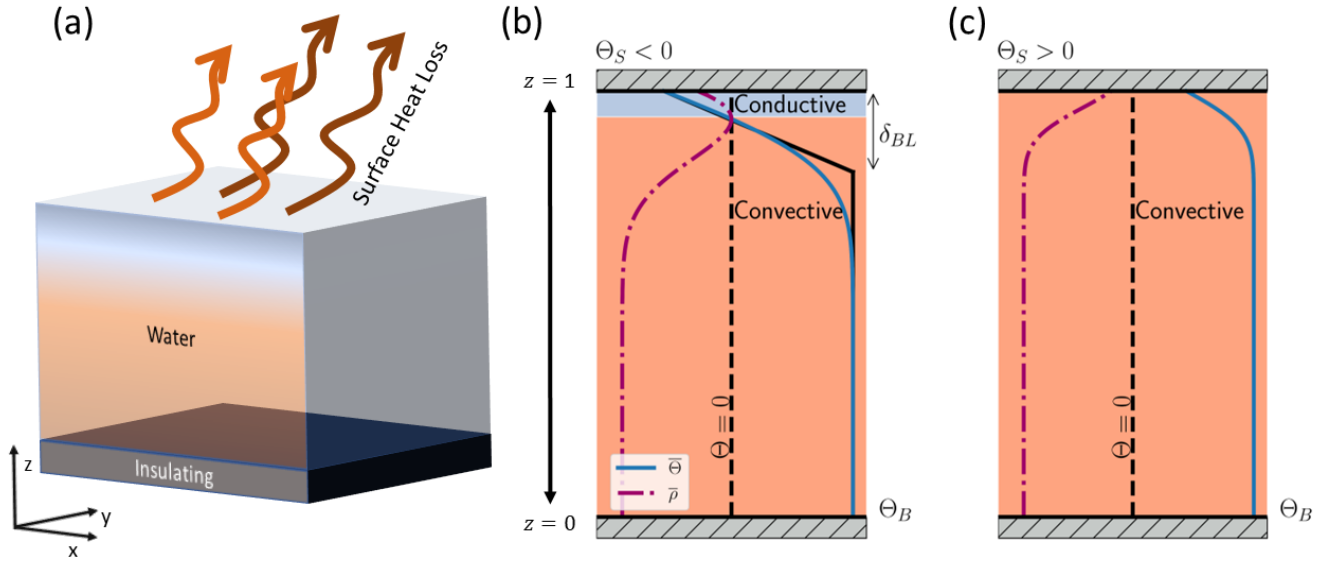


FIG. 1. (a) A schematic of the numerical domain. Diagram of the thermal structure within the domain for (b) $T_S < 0$ and (c) $T_S > 0$. An approximate piecewise-linear temperature profile is illustrated as a black line in (b). This figure is adapted from Olsthoorn et al. [6].

II. PROBLEM SETUP

We consider direct numerical simulations of a three-dimensional fluid domain with an initial uniform water temperature above \tilde{T}_{md} . The surface temperature boundary condition is given in (1), and the bottom boundary condition is insulating. Simulations were performed with the spectral solver SPINS [8], using pseudospectral spatial derivatives and a third-order time-stepping scheme. The horizontal domain is periodic and a Chebyshev grid is used in the vertical to resolve the top thermal boundary layer. Due to a limitation of the numerical code, both the top and bottom boundary conditions are no-slip. However, we do not believe that this will substantially affect our conclusions as our results from Regime I (when the surface temperature is above \tilde{T}_{md}) are similar to those found in Olsthoorn [5], which use a free-slip surface velocity condition, and Clarté et al. [3]. Figure 1a is a diagram of the problem setup.

Similar to the work of Olsthoorn et al. [6], we nondimensionalize the system by considering the domain depth H , the temperature difference $\Delta\tilde{T} = \tilde{T}_{md} - \tilde{T}_R$, the timescale of thermal diffusion $\tau_\kappa = \frac{H^2}{\kappa}$ and the corresponding velocity scale $\frac{H}{\kappa}$, where κ is thermal diffusivity. The equations of motion for nondimensional velocity \mathbf{u} and temperature Θ are then written

$$\left(\frac{\partial}{\partial t} + \mathbf{u} \cdot \nabla\right) \mathbf{u} = -\nabla P + \text{Ra}_0 \text{Pr} \Theta^2 \hat{\mathbf{k}} + \text{Pr} \nabla^2 \mathbf{u}, \quad (2)$$

$$\left(\frac{\partial}{\partial t} + \mathbf{u} \cdot \nabla\right) \Theta = \nabla^2 \Theta, \quad \nabla \cdot \mathbf{u} = 0. \quad (3)$$

We have defined the Rayleigh number (Ra_0), Prandtl number (Pr), and nondimensional temperature (Θ) as

$$\text{Ra}_0 = g C_T \Delta\tilde{T}^2 \frac{H^3}{\kappa \nu}, \quad \text{Pr} = \frac{\nu}{\kappa}, \quad \Theta = \frac{\tilde{T} - \tilde{T}_{md}}{\Delta\tilde{T}}, \quad (4)$$

where ν is the molecular viscosity of water, C_T is the thermal expansion coefficient for a quadratic equation of state, and g is the gravitational acceleration. We fixed $\text{Pr}=9$. In this scaling, \tilde{T}_{md} corresponds to $\Theta = 0$. Further, we can then rewrite the surface boundary conditions as

$$\frac{\partial \Theta}{\partial z} = -\beta (\Theta + 1), \quad z = 1, \quad (5)$$

with the Biot number β ,

$$\beta = \frac{\gamma H}{c_p \rho_0 \kappa}, \quad (6)$$

where c_p is the heat capacity of water and ρ_0 is a reference density. The Biot number β controls the relationship between the surface temperature and the convective flux through the water. We can see this relationship by rearranging equation (5) as

$$\Theta = -1 - \frac{1}{\beta} \frac{\partial \Theta}{\partial z}, \quad z = 1. \quad (7)$$

We find that the work of Olsthoorn et al. [6], which considered a fixed surface temperature condition, reduces to the limiting cases where $\beta \rightarrow \infty$. Conversely, for finite values of $\beta > 0$, the surface temperature is modified by the convective heat flux to the water surface. As the strength of the convection is determined, in part, by the surface temperature, the system naturally tends towards a dynamic equilibrium between the surface and bottom water temperatures.

In [6], the Authors showed that when the mean surface water temperature (Θ_S) decreases below \tilde{T}_{md} ($\Theta_S < 0$), there exists a stable (conductive) layer at the upper boundary, above a convective layer below (see Figure 1b). This is a result of the quadratic equation of state where the decreasing temperature with height results in a decreasing density profile near the surface. However, for finite β , the surface temperature depends upon the flux of heat to the surface and can result in a surface temperature above \tilde{T}_{md} ($\Theta_S > 0$). In this case, the entire domain is unstably stratified (see Figure 1c). This permits a free-convection regime without any stable layer.

Based upon the previous work of Olsthoorn [5] and Olsthoorn et al. [6], we expect there to exist three different convective regimes in this system:

- (I) $\Theta_S > 0$ - **Free-convection** without an upper conductive layer
- (II) $\Theta_S < 0$ and $\Theta_B > -C_3\Theta_S$ - **Penetrative-convection** with an upper conductive layer and strong convection below,
- (III) $\Theta_S < 0$ and $\Theta_B < -C_3\Theta_S$ - **Decaying-convection** with an upper conductive layer and weak/decaying convection below.

As we will see below, it is possible for the convective system to progress through each of these regimes as the mean water temperature decreases.

A. Simulated Cases

We performed a series of numerical simulations with a quadratic equation of state at different Rayleigh numbers and β values (see Table I). We initially perturb the three velocity components with a random perturbation sampled from a Normal distribution scaled by 10^{-2} . The numerical resolution ($N_x \times N_y \times N_z$) is similar to those of Olsthoorn et al. [6] and Olsthoorn [5], such that $\max \Delta \mathbf{x} < 3\eta_B$, where we compute the Batchelor scale $\eta_B = (\bar{\epsilon})^{-\frac{1}{4}} \text{Pr}^{-\frac{1}{2}}$, for horizontally averaged viscous dissipation rate $\bar{\epsilon}$ and grid spacing $\Delta \mathbf{x}$. Similarly, we ensure that $N_B \geq 10$ grid points over the thermal boundary layer, defined by $\delta_{BL} = \frac{\Theta_S - \Theta_B}{\frac{\partial \Theta}{\partial z}(z=1)}$. Table values are reported after the initial instability and the system has reached quasi-steady state with a finite δ_{BL} .

The domain width (L_x), depth (L_y), and height (L_z) were selected to have a large aspect ratio of four. At higher Ra_0 , limited computational resources forced us to reduce the aspect ratio to two. The results are consistent between the different Ra_0 cases.

III. RESULTS

After an initial transient, the surface-driven convection mixes the interior water to depth (see Figure 1b,c). We denote this near-uniform bottom water temperature Θ_B , which we calculate as a mean temperature below the mid-depth. Figure 2a is a plot of the mean surface temperature Θ_S and bottom temperature Θ_B for Case 8 ($\text{Ra}_0 = 9.0 \times 10^6, \beta = 25$). This case is presented as it demonstrates the three thermal regimes listed above. The convection initially drives the surface water above \tilde{T}_{md} ($\Theta_S > 0$). However, as Θ_B decreases, the convection weakens and the surface temperature drops below zero near $t \approx 0.01$. The penetrative-convection continues until Θ_B approaches zero and the decaying-convection regime starts around $t \approx 0.04$.

The rate at which the water temperature (Θ_B) decreases is determined by the flux of heat through the water surface (F). Similar to Olsthoorn et al. [6], we model the mean temperature profile as piecewise linear (see Figure 1b).

Case	Ra	β	Resolution ($N_x \times N_y \times N_z$)	Domain Size ($L_x \times L_y \times L_z$)	$\max \Delta \mathbf{x} / \eta_B$	N_B
1	9×10^5	1	$128 \times 128 \times 128$	$4 \times 4 \times 1$	1.472	20
2	9×10^5	10	$256 \times 256 \times 256$	$4 \times 4 \times 1$	1.098	37
3	9×10^5	25	$256 \times 256 \times 256$	$4 \times 4 \times 1$	1.165	36
4	9×10^5	100	$256 \times 256 \times 256$	$4 \times 4 \times 1$	1.190	37
5	9×10^5	1000	$256 \times 256 \times 256$	$4 \times 4 \times 1$	1.163	38
6	9×10^6	1	$128 \times 128 \times 128$	$4 \times 4 \times 1$	2.800	17
7	9×10^6	10	$512 \times 512 \times 256$	$4 \times 4 \times 1$	1.206	29
8	9×10^6	25	$512 \times 512 \times 256$	$4 \times 4 \times 1$	1.406	28
9	9×10^6	100	$512 \times 512 \times 256$	$4 \times 4 \times 1$	1.565	28
10	9×10^6	1000	$512 \times 512 \times 256$	$4 \times 4 \times 1$	1.662	27
11	9×10^7	25	$512 \times 512 \times 256$	$2 \times 2 \times 1$	1.592	21
12	9×10^7	100	$512 \times 512 \times 256$	$2 \times 2 \times 1$	1.918	20

TABLE I. Table of the parameters for each numerical simulation. Note that the domain width for $Ra_0 = 9 \times 10^7$ is half of the other cases. We report the maximum grid spacing relative to the Batchelor scale (η_B) defined based upon horizontally averaged dissipation rates. We further report the number of grid points within the surface boundary layer (N_B) defined based upon the surface temperature gradient. Both η_b and N_B are calculated after the initial onset of convection.

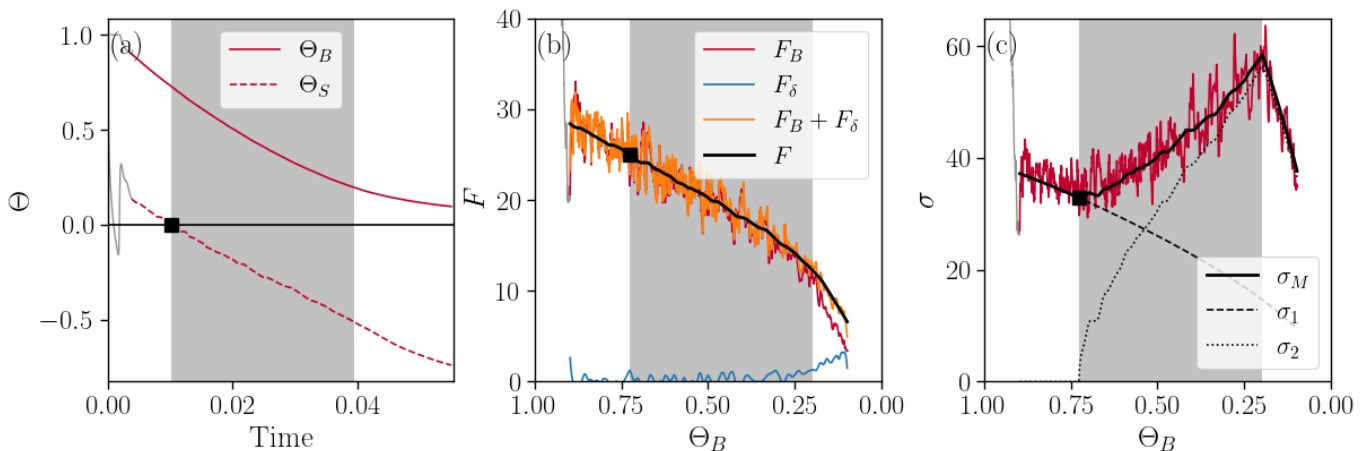


FIG. 2. (a) A plot of the time evolution of mean bottom water temperature Θ_B and surface water Θ_S . Here and elsewhere, the initial transient is included as light-grey line. (b) The simulated surface heat flux (F) as a function of bottom water temperature Θ_B . (c) The temperature decay rate σ as a function of Θ_B . A black dot denotes where $\Theta_S = 0$, and the penetrative-regime (Regime II) is denoted by the grey banner.

Computing the time-derivative of this profile, we can show that

$$F \approx \underbrace{-\frac{d\Theta_B}{dt}}_{F_B} - \underbrace{\frac{d}{dt} \left(\left(\frac{\Theta_S - \Theta_B}{2} \right) \delta_{BL} \right)}_{F_\delta}. \quad (8)$$

The surface cooling is the sum of two components: the cooling of the bottom water (F_B) and the growth of the thermal boundary layer (F_δ). At high Ra_0 , when the convection is vigorous, the boundary layer thickness is small and the surface flux is dominated by decreasing Θ_B ($F \sim F_B, F_B \gg F_\delta$). When convection weakens ($\Theta_B \rightarrow 0$), as in the decaying-convection regime, a significant portion of the surface heat loss is used to grow the top boundary layer ($F_\delta > 0, F_\delta \sim F_B$). Looking at Figure 2b, we observe a growth in F_δ when $\Theta_B \approx 0.2$, which, as we discuss below, occurs at the transition to the decaying-convection regime.

A. How rapidly does the water temperature decrease?

We can quantify how quickly the mean water temperature decreases through the decay rate σ , which quantifies the rate at which the temperature approaches an equilibrium value. When $\Theta_S > 0$, convection will drive the mean water temperature to the mean surface temperature ($\Theta_B \rightarrow \Theta_S$). However, when $\Theta_S < 0$, convection will only decrease the mean water temperature to the temperature of maximum density ($\Theta \rightarrow 0$). We quantify the rate at which Θ_B approaches equilibrium as the decay rate

$$\sigma = \frac{-1}{\Theta_B - \Theta_0} \frac{d\Theta_B}{dt}, \quad (9)$$

where $\Theta_0 = \max\{\Theta_S, 0\}$. As can be shown from (8), where $F_\delta \ll 1$, σ is equivalent to the Nusselt number. Thus, as suggested by Olsthoorn [5] and others, we would expect that for free convection, σ should scale with the surface-temperature-dependant Rayleigh number $\text{Ra}_e = \text{Ra}_0 (\Theta_B - \Theta_0)^2$,

$$\sigma_1 \sim C_1 \text{Ra}_e^p, \quad \Theta_S > 0. \quad (10)$$

However, the work of Olsthoorn et al. [6] suggests that for $\Theta_S < 0$, two different thermal regimes are possible with different decay rates:

$$\sigma_2 \sim C_2 (\text{Ra}_0 \Theta_S^2)^p \begin{cases} 1, & \Theta_B \geq -C_3 \Theta_S \\ \left(\frac{\Theta_B}{C_3 \Theta_S}\right)^{2p}, & \Theta_B < -C_3 \Theta_S \end{cases}, \quad \Theta_S < 0, \quad (11)$$

where we have modified the model of Olsthoorn et al. [6] to account for the changing surface temperature.

Figure 2c is a plot of the numerically computed σ compared with σ_1 and σ_2 . Similar to the values of [5, 6], we fit $C_1 = 0.28, p = 0.31, C_2 = 0.6, C_3 = 0.385$. We find that σ_1 agrees well with the simulated σ during the free-convection regime $\Theta_S > 0$ and that σ_2 agrees well during the decaying-convection regime, but neither agree well during the penetrative-convection regime (see the grey shaded region in Figure 2).

We can approximate the decay rate over the entire simulation by considering both contributions to the temperature decrease as

$$\sigma_M = \sqrt{\sigma_1^2 + \sigma_2^2}, \quad (12)$$

which is essentially the norm of two orthogonal contributions to the temperature decay rate. We find good agreement between this combined model (σ_M) and the simulated temperature decay (σ) across all three temperature regimes (Figure 2c).

Further this combined model agrees with all of the simulated cases (See figure 3). Despite the complexity of this model, and the significant oscillations, this model captures the temperature decay rate through all three identified thermal regimes.

B. When do the regime transitions occur?

It is import to note that the decay rate σ is itself a function of both Θ_B and Θ_S . Thus, we need additional information to predict Θ_S given measurements of Θ_B (or vice versa). We have shown (Figure 2b) that except during the decaying-convection regime (where the boundary layer grows relatively rapidly), the surface flux is well approximated by $F \approx -\sigma_M (\Theta_B - \Theta_0)$. Further, following the approach of Olsthoorn [5], we can use the surface boundary condition (5) to determine

$$\sigma_M(\Theta_B, \Theta_S; \text{Ra}_0) (\Theta_B - \Theta_0) = \beta (\Theta_S + 1). \quad (13)$$

We further isolate a factor of Ra_0^p from σ_M to rewrite

$$\frac{\text{Ra}_0^p}{\beta} = \frac{1}{\Gamma_M(\Theta_B, \Theta_S)} \left(\frac{(\Theta_S + 1)}{(\Theta_B - \Theta_0)} \right), \quad \Gamma(\Theta_B, \Theta_S) = \frac{\sigma_M(\Theta_B, \Theta_S; \text{Ra}_0)}{\text{Ra}_0^p}. \quad (14)$$

The scaled decay rate Γ_M is independent of the Rayleigh number. That is, for any value of Θ_S , we have identified an implicit equation to determine Θ_B (or vice versa), with the key parameter Ra_0^p/β .

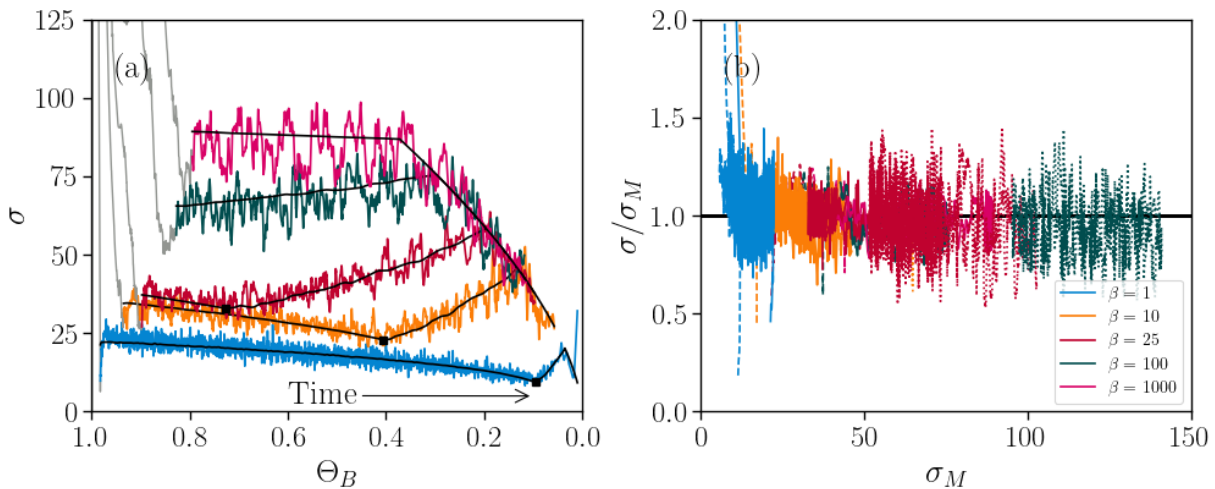


FIG. 3. (a) Plot of the compute decay rate σ vs. Θ_B for the cases $Ra_0 = 9 \times 10^6$. The combined model σ_M is included as a black line. (b) Comparison of the computed σ vs. σ_M for all simulated cases. The model σ_M is given in (12) with fit parameters $C_1 = 0.28, p = 0.31, C_2 = 0.6, C_3 = 0.385$. Note that data from $\Theta_B < 0.01$ was removed.

We demonstrate the validity of this model by investigating the evolution of Θ_S as a function of Θ_B . Figure 4a is a plot of Θ_S as a function of Θ_B for different values of β with $Ra_0 = 9 \times 10^6$. For a given value of $\Theta_B = 0.5$, we find good agreement between the predicted values of Θ_S from (14) and those found in the simulations (Figure 4b).

We have identified three key convective regimes in this system. The regime transition between Regime I (free-convection) and Regime II (penetrative-convection) occurs when $\Theta_S = 0$; when the surface temperature equals the temperature of maximum density. The second regime transition between Regime II (penetrative-convection) and Regime III (decaying-convection) occurs when $\Theta_B = -C_3\Theta_S$; when the convection significantly weakens and the thermal boundary layer grows rapidly. Given the physical parameters of this system, we can use (14) to determine the critical values of Θ_B when these transitions are expected to occur. Figure 4c includes a comparison of the predicted and simulated points of transition. We find that the model is reasonable at predicting these transitions, though we note that the value of Θ_B for $\Theta_S = 0$ is slightly under predicted.

IV. DISCUSSION AND CONCLUSION

The dynamic surface boundary condition (5) prescribes how the heat flux through the surface is coupled to the surface water temperature. In a cooling system, like the one described here, the atmospheric forcing cools the surface, which drives convection. However, the induced convection in the water results in a net-positive vertical heat flux, which warms the surface from below, increasing the surface temperature. That is, there is a dynamic equilibrium for the surface temperature as it both generates, and is modulated by, the convection.

The boundary condition (5) can be viewed as a parameterization for the finite conductivity of the atmospheric boundary layer above the water. This is similar to the significant body of literature discussing the role of the finite conductivity of the bounding plates used in experimental studies of Rayleigh-Bénard convection. For example, Chillà et al. [2] argue it is the finite conductivity of the bounding plates that explain why the ‘ultimate’-convective regime is not found in certain experiments. Verzicco [9] and Brown et al. [1] determine correction factors to account for this finite conductivity, assuming a linear equation of state. Wittenberg [13] further discusses the role of β on heat flux bounds across the whole liquid/solid-boundary system. This present paper focuses on the role of the nonlinear equation of state in modifying the temperature evolution of the system.

The present manuscript builds upon these previous studies to investigate convection with a quadratic equation of state and has revealed three convective regimes: Regime I free-convection, Regime II penetrative-convection, and Regime III decaying-convection (See figure 2). The boundaries between these regimes are then determined where $\Theta_S = 0$ (Regime I to Regime II) and where $\Theta_B = -C_3\Theta_S$ (Regime II to Regime III). The critical values of Θ_B can be estimated from (14). For a known Θ_B , such as from field measurements, (14) can be further used to estimate the corresponding surface temperature.

One of the aims of this work is to determine when we expect to find ice-formation as a function of Θ_B . These direct numerical simulations are not capable of including a freezing surface flux, but, as shown by [12], the shape of

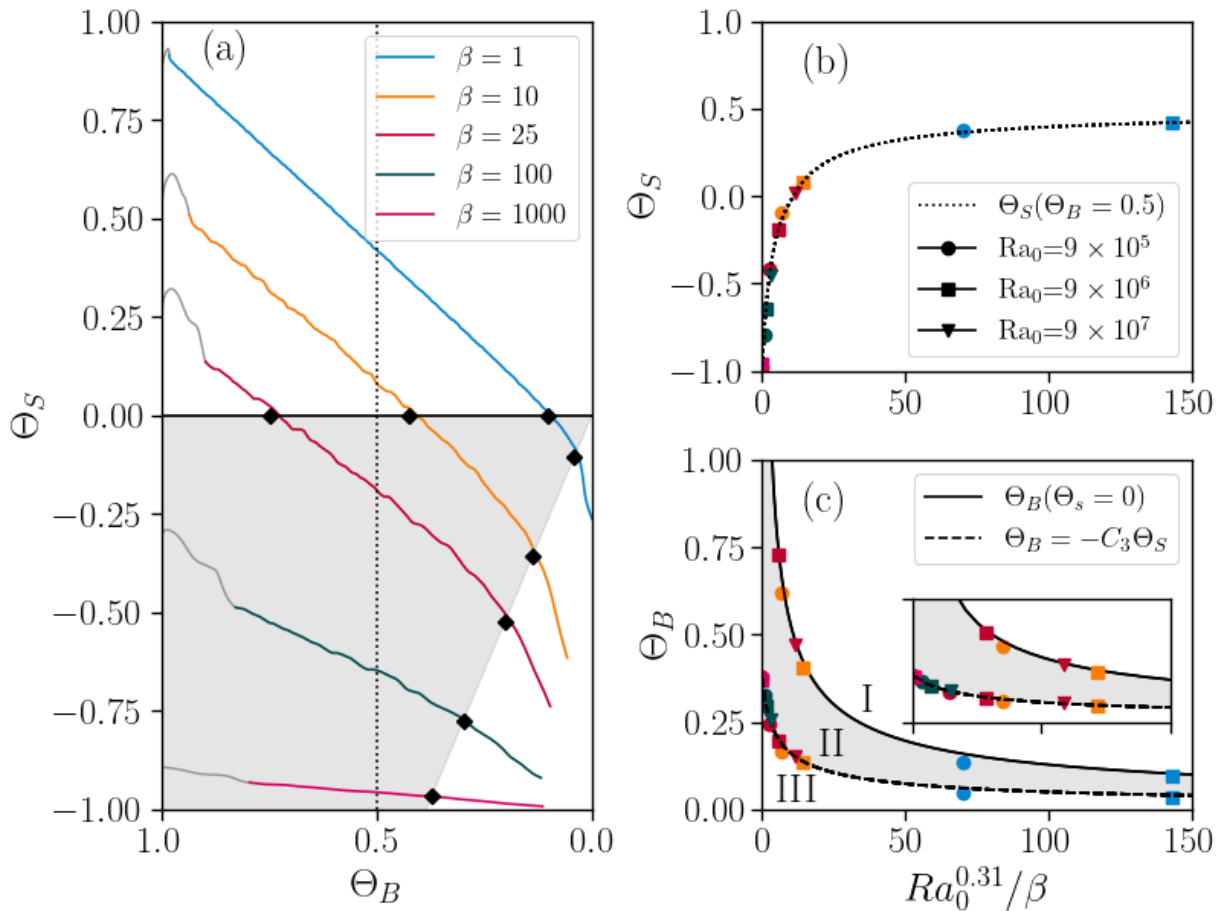


FIG. 4. (a) Surface temperature (Θ_S) vs. bottom temperature (Θ_B) for $Ra_0 = 9 \times 10^6$. Black diamonds denote the predicted regime transitions for each case when $\Theta_S = 0$ and when $\Theta_B = -C_3\Theta_S$. (b) The surface temperature Θ_S for a picked value of $\Theta_B = 0.5$ (corresponding to the vertical dotted line in (a)). (c) The bottom temperature Θ_B at the regime boundaries ($\Theta_S = 0$ and $\Theta_B = -C_3\Theta_S$) as a function of $Ra_0^{0.31}/\beta$. The regimes are denoted (I) free-convection regime, (II) penetrative-convection regime [shaded grey], and (III) decaying-convection regime. The inset presents the same data on a reduced x-axis of $Ra_0^{0.31}/\beta = [0, 20]$.

the ice is determined by the water convection. Future work would include an ice-growth model to predict the timing and growth of ice formation. That said, in the absence of external forcing, we would expect that the water surface will start to freeze once its temperature is cooled below the freezing point. Due to the rapidly decreasing surface heat flux, we hypothesize that ice formation will occur shortly after the transition from regime (II) to regime (III). Future work will investigate how these regimes would be updated in the presence of wind-driven mixing, and if the regime transitions can be identified in field measurements.

ACKNOWLEDGEMENTS

We want to thank Dan Robb and Ted Tedford for their feedback on this work. This work was funded in part by the Natural Sciences and Engineering Research Council of Canada. Computational support was provided by the Queen's University Centre for Advanced Computing.

[1] E. Brown, A. Nikolaenko, D. Funfschilling, and G. Ahlers. Heat transport in turbulent Rayleigh-Bénard convection: Effect of finite top- and bottom-plate conductivities. *Physics of Fluids*, 17(7):075108, July 2005. ISSN 1070-6631, 1089-7666. doi:10.1063/1.1964987. URL <http://aip.scitation.org/doi/10.1063/1.1964987>.

- [2] F. Chillà, M. Rastello, S. Chaumat, and B. Castaing. Ultimate regime in Rayleigh–Bénard convection: The role of plates. *Physics of Fluids*, 16(7):2452–2456, July 2004. ISSN 1070-6631, 1089-7666. doi:10.1063/1.1751396. URL <http://aip.scitation.org/doi/10.1063/1.1751396>.
- [3] T. T. Clarté, N. Schaeffer, S. Labrosse, and J. Vidal. The effects of a Robin boundary condition on thermal convection in a rotating spherical shell. *Journal of Fluid Mechanics*, 918:A36, July 2021. ISSN 0022-1120, 1469-7645. doi:10.1017/jfm.2021.356. URL https://www.cambridge.org/core/product/identifier/S0022112021003566/type/journal_article.
- [4] J. Hitchen and A. J. Wells. The impact of imperfect heat transfer on the convective instability of a thermal boundary layer in a porous media. *Journal of Fluid Mechanics*, 794:154–174, May 2016. ISSN 0022-1120, 1469-7645. doi:10.1017/jfm.2016.149. URL https://www.cambridge.org/core/product/identifier/S002211201600149X/type/journal_article.
- [5] J. Olsthoorn. Accounting for surface temperature variations in Rayleigh–Bénard convection. *Physical Review Fluids*, 8(3):033501, Mar. 2023. ISSN 2469-990X. doi:10.1103/PhysRevFluids.8.033501. URL <https://link.aps.org/doi/10.1103/PhysRevFluids.8.033501>.
- [6] J. Olsthoorn, E. W. Tedford, and G. A. Lawrence. The cooling box problem: convection with a quadratic equation of state. *Journal of Fluid Mechanics*, 918:A6, July 2021. ISSN 0022-1120, 1469-7645. doi:10.1017/jfm.2021.319. URL https://www.cambridge.org/core/product/identifier/S0022112021003190/type/journal_article.
- [7] M. Plumley and K. Julien. Scaling Laws in Rayleigh–Bénard Convection. *Earth and Space Science*, 6(9):1580–1592, Sept. 2019. ISSN 2333-5084, 2333-5084. doi:10.1029/2019EA000583. URL <https://onlinelibrary.wiley.com/doi/abs/10.1029/2019EA000583>.
- [8] C. J. Subich, K. G. Lamb, and M. Stastna. Simulation of the Navier–Stokes equations in three dimensions with a spectral collocation method. *International Journal for Numerical Methods in Fluids*, 73(2):103–129, Sept. 2013. ISSN 0271-2091, 1097-0363. doi:10.1002/flid.3788. URL <https://onlinelibrary.wiley.com/doi/10.1002/flid.3788>.
- [9] R. Verzicco. Effects of nonperfect thermal sources in turbulent thermal convection. *Physics of Fluids*, 16(6):1965–1979, June 2004. ISSN 1070-6631, 1089-7666. doi:10.1063/1.1723463. URL <http://aip.scitation.org/doi/10.1063/1.1723463>.
- [10] Q. Wang, Q. Zhou, Z.-H. Wan, and D.-J. Sun. Penetrative turbulent Rayleigh–Bénard convection in two and three dimensions. *Journal of Fluid Mechanics*, 870:718–734, July 2019. ISSN 0022-1120, 1469-7645. doi:10.1017/jfm.2019.286. URL https://www.cambridge.org/core/product/identifier/S0022112019002866/type/journal_article.
- [11] Q. Wang, P. Reiter, D. Lohse, and O. Shishkina. Universal properties of penetrative turbulent Rayleigh–Bénard convection. *Physical Review Fluids*, 6(6):063502, June 2021. ISSN 2469-990X. doi:10.1103/PhysRevFluids.6.063502. URL <https://link.aps.org/doi/10.1103/PhysRevFluids.6.063502>.
- [12] Z. Wang, E. Calzavarini, C. Sun, and F. Toschi. How the growth of ice depends on the fluid dynamics underneath. *Proceedings of the National Academy of Sciences*, 118(10):e2012870118, Mar. 2021. doi:10.1073/pnas.2012870118. URL <https://www.pnas.org/doi/full/10.1073/pnas.2012870118>. Publisher: Proceedings of the National Academy of Sciences.
- [13] R. W. Wittenberg. Bounds on Rayleigh–Bénard convection with imperfectly conducting plates. *Journal of Fluid Mechanics*, 665:158–198, Dec. 2010. ISSN 0022-1120, 1469-7645. doi:10.1017/S0022112010003897. URL https://www.cambridge.org/core/product/identifier/S0022112010003897/type/journal_article.
- [14] B. Yang, M. G. Wells, J. Li, and J. Young. Mixing, stratification, and plankton under lake-ice during winter in a large lake: Implications for spring dissolved oxygen levels. *Limnology and Oceanography*, 65(11):2713–2729, Nov. 2020. ISSN 0024-3590, 1939-5590. doi:10.1002/lno.11543. URL <https://onlinelibrary.wiley.com/doi/10.1002/lno.11543>.
- [15] B. Yang, M. G. Wells, B. C. McMeans, H. A. Dugan, J. A. Rusak, G. A. Weyhenmeyer, J. A. Brenttrup, A. R. Hrycik, A. Laas, R. M. Pilla, J. A. Austin, P. J. Blanchfield, C. C. Carey, M. M. Guzzo, N. R. Lottig, M. D. MacKay, T. A. Middel, D. C. Pierson, J. Wang, and J. D. Young. A New Thermal Categorization of Ice-Covered Lakes. *Geophysical Research Letters*, 48(3), Feb. 2021. ISSN 0094-8276, 1944-8007. doi:10.1029/2020GL091374. URL <https://onlinelibrary.wiley.com/doi/10.1029/2020GL091374>.